In Vitro and In Vivo Characteristics of [Iodine-125] 3-(R)-Quinuclidinyl (S)-4-Iodobenzilate

Raymond E. Gibson, Timothy A. Schneidau, Victor I. Cohen, Virendar Sood, Jennifer Ruch, John Melograna, William C. Eckelman,* and Richard C. Reba

Radiopharmaceutical Chemistry, George Washington University Medical Center, Washington, DC

The radioiodinated muscarinic acetylcholine receptor antagonist, [^{125}I] 3-quinuclidinyl 4-iodobenzilate, has two high affinity diastereomeric forms, the (R,R) and (R,S)-isomers. The (R,S)-diastereomer is only threefold lower in affinity than the (R,R)-isomer, but the kinetic properties are considerably different—the dissociation rate constant is 13-fold faster for the (R,S)-isomer and the association rate constant is two to threefold faster. The calculated affinity is therefore only fourfold lower. In vivo, the clearance of (R,S)-4IQNB from receptor-rich tissue is also more rapid than that of the (R,R)-isomer, that is a reflection of the more rapid in vitro kinetic properties since the physicochemical properties and the metabolic clearance of the diastereomers is the same.

J Nucl Med 30:1079–1087, 1989

3-Quinuclidinyl 4-iodobenzilate (4IQNB: Fig. 1) is a high affinity muscarinic acetylcholine receptor (m-AChR) antagonist. It has been labeled with iodine-125 (^{125}I) and iodine-123 (^{123}I) with high specific activity (*1*) and the in vivo distribution is consistent with receptor mediated localization in the central nervous system (CNS) (*2*). As such we have used [^{123}I]4IQNB to obtain images of the receptor distribution in the CNS of man (*3*) and find that images obtained from patients with Alzheimer's disease exhibit lower concentrations of radioactivity in the temperoparital cortex compared to healthy individuals (*4*). The parent structure, 3-quinuclidinyl benzilate, exhibits stereoisomerism about the 3-carbon atom in the quinuclidine portion of the molecule (single asterisk in Fig. 1), and the (R)-isomer of QNB is at least 100-fold higher in affinity as compared to the (S)-isomer (*5*). Therefore, we have used the (S)-isomer of 4IQNB to determine the nonreceptor interactions of the radioligand since the physicochemical properties of the (R)- and (S)-isomers are similar but the (S)-isomer will exhibit minimal receptor-specific interactions (*6,7*). The addition of an iodine to one of the phenyl rings in QNB introduces a second site of stereoisomerism (double asterisk in Fig. 1). The introduction of a second chiral carbon produces four diastereomers and it is likely that (R,R)- and (R,S)-4IQNB will exhibit different affinities for the m-AChR; when the ester moiety is optically active, the (R)-configuration is more potent than the (S)-configuration (*8*). The imaging studies conducted in human subjects used the most active isomer [^{123}I] (R,R)-4IQNB. The existence of a diastereomer which exhibits different binding properties from the (R,R)-diastereomer provides the opportunity to evaluate methods for receptor-quantification, e.g., the physicochemical properties of the (R,S)-diastereomer are identical to that of the (R,R)-diastereomer and the difference in the in vivo pharmacokinetic behavior should therefore be related to the intrinsic kinetic parameters. We have therefore prepared (R)-3-quinuclidinyl (S)-4-iodobenzilate [(R,S)-4IQNB] and describe herein its in vitro and in vivo characteristics.

Received Sept. 8, 1988; revision accepted Jan. 9, 1989.

For reprints contact: Raymond E. Gibson, MD, Research Imaging, Merck, Sharp and Dohme Research Laboratories, WP-44C, West Point, PA 19486.

* Present address: The Squibb Institute for Medical Research, New Brunswick, NJ.

MATERIALS AND METHODS

Radioligands

To obtain the pure diastereomers, we first prepared 4-nitrobenzilic acid as previously described (*1*). The (S)-stereoisomer is obtained by repeated recrystallization with quinine

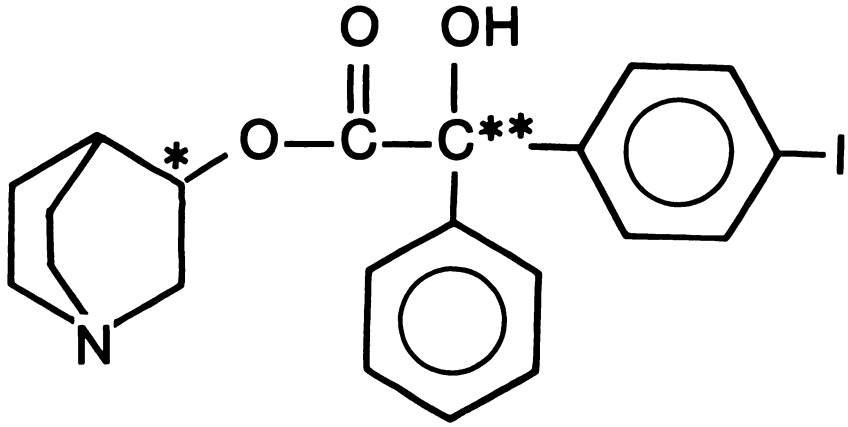

FIGURE 1
Structure of 3-quinuclidinyl 4-iodobenzilate indicating sites of stereoisomerism. In the quinuclidinyl moiety, the (R)-isomer (*) is more active than the (S). Iodination of one phenyl ring creates a second chiral carbon (**).

(*9*). After five recrystallizations, the optical rotation remained constant with the value of $[\alpha]_D^{24}$ of −76.2°. The acid was esterified with ethanol followed by transesterification with (R)-3-quinuclidinol as previously described (*1,9*). The nitro group was catalytically reduced using palladium on polyethylene and the triazene intermediate was obtained by reaction of 5-methylpiperidine with the diazonium salt prepared from 3-quinuclidinyl (S)-4-aminobenzilate as previously described (*1,9*). (R)-4-nitrobenzilic acid was isolated by multiple recrystallization of the quinidine salt (*9*). After four recrystallizations, the optical rotation was constant at $[\alpha]_D^{24}$ = +121.2°. The subsequent conversion to (R)-3-quinuclidinyl (R)-4-triazenobenzilate was achieved as described for the (R,S)-isomer (*9*).

The radioiodinated product was obtained by the reaction of [^{125}I] NaI with the triazene in strong acid (*1,9*). The product was purified by high performance liquid chromatography using a carbon-18 reversed-phase column eluted with 60:40 methanol:water containing 10 m*M* formic acid and 1% octane sulfonic acid. The fractions which corresponded to the elution volume of (R,S)-4IQNB were pooled and evaporated to dryness in vacuo. The octane sulfonic acid was neutralized with 5% $NaHCO_3$, and the free base extracted in ethyl acetate. The solvent is removed in vacuo and the radioligand reconstituted in 95% EtOH. The yield for the [^{125}I] (R,S)-4IQNB is 13.4% (± 1.9%, n = 20), and for the (R,R)-isomer is 15.5% (± 1.1%, n = 80). The radiochemical purity was >98% at the end of synthesis and can be stored at −70° C for 6 mo maintaining radiochemical purity >95%. The specific activities for [^{125}I] (R,S)- and (R,R)-4IQNB are 1,172 Ci/mmol (n = 14) and 1,087 Ci/mmol (n = 9), respectively (*9*). Hydrogen-3 (−)-3-quinuclidinyl benzilate (QNB) is commercially available (DuPont Company, No. Billerica, MA) (32 Ci/mmol).

In Vitro Binding Assays

The kinetics of radioligand interaction with the m-AChR from corpus striatum and the equilibrium binding were determined as previously described (*2,10*). Values for parameters are the average of at least five determinations. The solid lines in Figures 2, 3, and 4 are the theoretic curves generated from the parameters cited in the legends to those figures. When the radioiodinated ligand has an effective specific activity less than theoretic, the association rate kinetics are complex if the unlabeled receptor-binding site-products exhibit kinetics properties which differ significantly from that of the radioiodinated ligand. This topic will be treated in detail in a separate manuscript.

In Vivo Studies

Five microcuries of [^{125}I] (R,S)-4IQNB and 5μCi of [^{3}H] QNB was coinjected into female Spraque-Dawley rats (200-250 g) via exposed femoral vein. Hydrogen-3 QNB was coinjected with the radioiodinated ligand to provide an internal control. Animals were killed at various times, organs of interest removed, biopsy samples obtained and solubilized in Protosol (DuPont). The samples were counted for ^{125}I in an autogamma counter and the radioactivity calculated using the absolute counting method of Eldridge and Crowther (*11*). Liquid scintillation cocktail was then added to the samples and they were counted in a liquid scintillation counter set for ^{3}H/^{125}I dual label counting. There were no significant differences between the results obtained for ^{125}I radioactivity by either method of counting. The results for the tissue distribution study are expressed as % injected dose per gram of tissue (wet weight).

To obtain plasma-activity time data, rats were injected with 100 μCi of either [^{125}I] (R,R)- or (R,S)-4IQNB, and blood samples taken from the orbital sinus at various times from 0 to 1,440 min. Samples were centrifuged at 5,000 rpm for 3 min, and the plasma thus obtained counted in an autogamma counter. To determine the metabolized fraction, the plasma was extracted with EtOAc, which provides the lipophilic fraction present in the plasma. To determine the presence of lipophilic metabolites that are extracted, rats were injected with 0.3 mCi of either diastereomer of the radioligand, the animals killed at 3 hr, and blood removed by cardiac puncture. The samples were treated as above but the ethyl acetate extract was chromatographed on silica gel in 2% NH_4OH in MeOH and the plates scanned for radioactivity.

For autoradiographic studies, 0.3 to 0.5 mCi of [^{125}I] (R,S)-4IQNB was injected via femoral vein and the rats killed at 1, 3, and 5 hr. The brains were rapidly removed and placed in powdered dry ice. Parasagittal sections were obtained which correspond to the lateral 1.9-mm section of Paxinos and Watson (*12*). Sections of 12-μm thickness were juxtaposed to H-3 sensitive film for various times (exposure time determined by the count rate per slice). The autoradiographs are presented for visual comparisons. Quantitative comparisons are obtained from autopsy samples presented in Table 2.

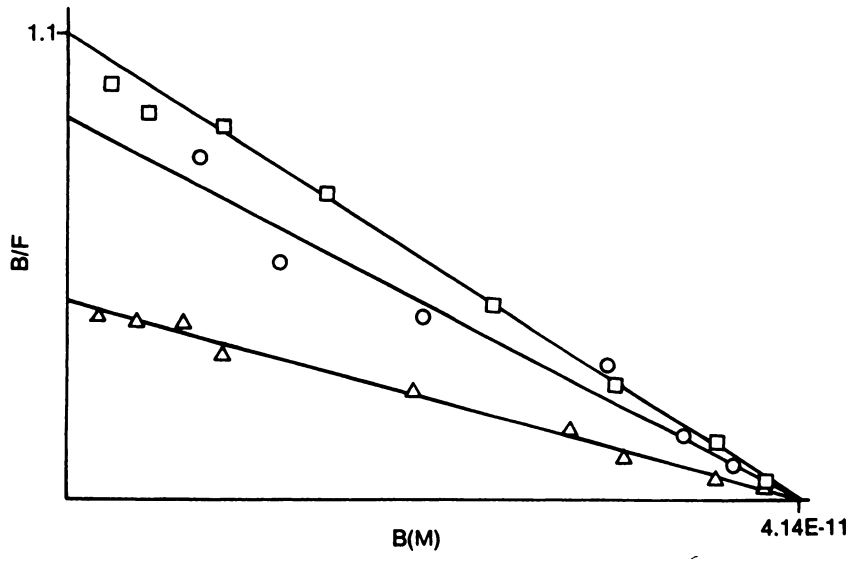

FIGURE 2
Scatchard analysis of the binding of [^{125}I] (R,S)-4IQNB (△), (R,R)-4IQNB (□) and [^{3}H] QNB (○) binding to m-AChR from corpus striatum. Representative curves from one study: (△) $K_A = 1.14 \times 10^{10}$ M^{-1} M, (□) 2.66×10^{10} M^{-1}, and (○) 2.18×10^{10} M^{-1}; statistics for multiple determinations of equilibrium association constants and specific activities are presented in the results section.

RESULTS

The ^{125}I (R,S)-diastereomeric isomer of 4IQNB has been prepared in specific activities of 1,100 Ci/mmol and with a high equilibrium association constant (Fig. 2). The affinity constant ($K_A = 2.9$ [± 0.45] $\times 10^9$ M^{-1}) is threefold lower than that of the (R,R)-diastereomer ($K_A = 8.9$ [± 1.4] $\times 10^9$ M^{-1}). Despite this small difference in affinity, the kinetics of dissociation are considerably different. Figures 3 presents the comparative dissociation-rate profile for (R,S)-4IQNB and (R,R)-4IQNB. The rate of dissociation of the (R,S)-diastereomer for m-AChR isolated from the corpus striatum ($k_{-1} = 0.0654 \pm 0.011$ min^{-1}, n = 9) is 13-fold more rapid than that of the R,R-isomer ($k_{-1} = 0.0049 \pm 0.0004$ min^{-1}, n = 19) (*9*). The calculated association rates for the (R,S)- and (R,R)-isomers, using $k_{+1} = K_A * k_{-1}$, are 1.9×10^8 $M^{-1}min^{-1}$ and 4.4×10^7 $M^{-1}min^{-1}$, respectively. We confirmed that the rate of association of (R,S)-4IQNB is 2.5-fold faster than that of (R,R)-4IQNB (Fig. 4).

The time course of the distribution of (R,S)-4IQNB is provided in Table 1 (systemic) and Table 2 (CNS). The highest concentrations of radiotracer are observed in the kidneys, adrenals, lung, and liver in the first 4 hr. Radioactivity clears rapidly from the myocardium as well as nontarget tissues such as ovaries, adrenals, and muscle. Radioactivity increases with time in the intestines, probably reflecting the metabolic fate of the radioligand. The radioactivity in the blood apparently

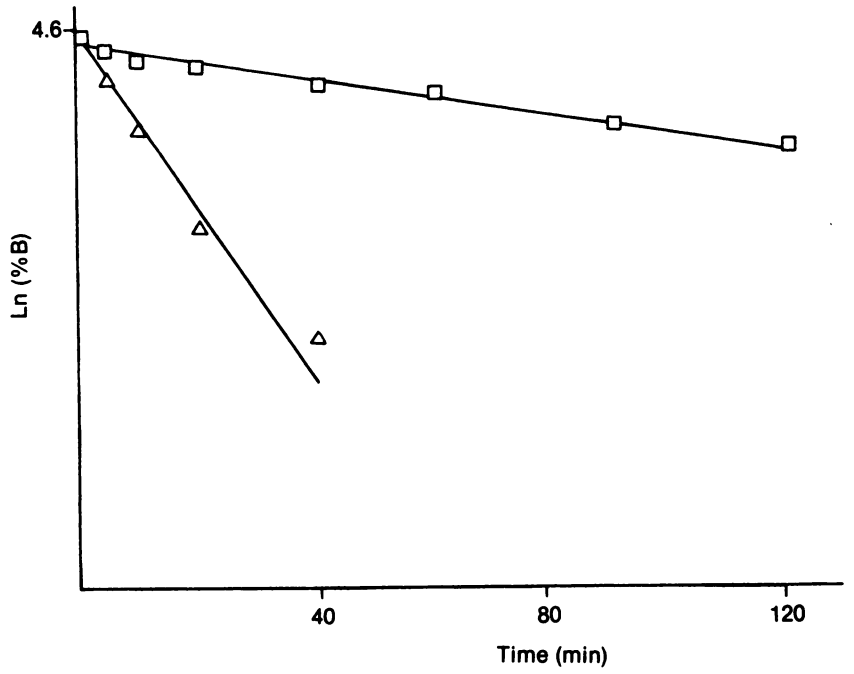

FIGURE 3
Dissociation of [^{125}I] (R,S)-4IQNB (△) and (R,R)-4IQNB (□) from m-AChR from corpus striatum. For the representative curves shown: $k_{-1} = 0.07$ min^{-1} (△) and 0.005 min^{-1} (□). Dissociation rates were determined as described in Ref. (*10*).

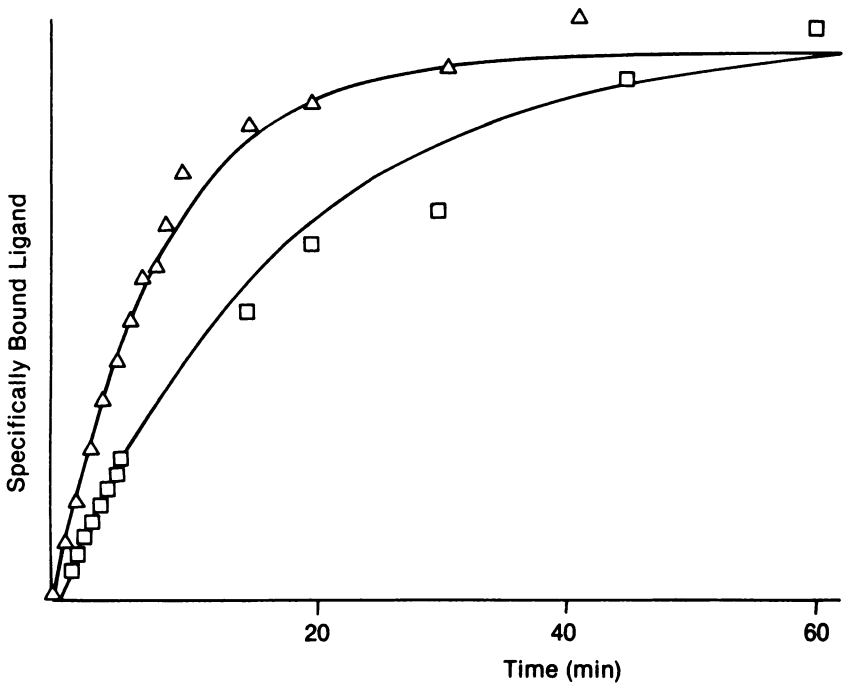

FIGURE 4
Association of [^{125}I] (R,S)-4IQNB (△) and (R,R)-4IQNB (□) to m-AChR from corpus striatum. Association rate constants obtained as described in Ref. (*10*). For the representative curves shown: $k_{+1} = 3.6 \times 10^8$ $M^{-1}min^{-1}$ (□) and 8.9×10^8 $M^{-1}min^{-1}$ (△).

increased from 15 to 30 min postinjection. This anomaly was not observed in studies to determine the plasma-radioactivity time-course. The systemic distribution of the (R,S)-isomer is similar to that of the (R,R)-isomer (*2*) with the exception that the radioactivity clears the heart more rapidly in the case of (R,S)-4IQNB. The distribution of radioactivity in the CNS during the first hour following i.v. injection of ^{125}I-labeled (R,S)-4IQNB is also similar to that reported for the (R,R)-isomer (*2*). However, the radioactivity clears the CNS structures more rapidly in the case of the (R,S)-isomer. By 4 hr, 75% of the radioactivity has washed out of the corpus striatum, the region with the highest concentration of m-AChR. In the in vivo distribution studies, [^{3}H] QNB was coinjected to provide an internal standard for comparison with earlier studies and it is clear that the clearance of QNB (parenthetical values in Table 1) is much slower than that of the (R,S)-4IQNB. As noted in our earlier studies on (R,R)-4IQNB, the concentration of label in the CNS is lower for the iodinated ligand than for the tritiated ligand (*2*). The concentration of muscarinic antagonists present when both radioligands are injected provides receptor occupancy <5% which indicates that both radiotracers will behave linearly with no interactions. The results presented in Table 2 for [^{3}H] QNB are consistent with results previously reported (*2*).

The distribution of radioactivity in various regions of the CNS was determined by the use of autoradiography. To visualize a greater number of structures per slice, we obtained sagittal slices from rat brain at various times after i.v. injection of (R,S)-4IQNB (Fig. 5). At 1 hr (Fig. 5A), the most heavily labeled structures are the cortex, hippocampus, corpus striatum, nucleus accumbens, olfactory nuclei, and the anteroventral (AV) nucleus of the thalamus. The remaining thalamic nuclei are labeled to a lesser extent, followed by the hypothalamus, brain stem, and cerebellum, all of which are very lightly labeled. By 3 hr (Fig. 5B), the highest concentrations of radioactivity are in the cortex, hippocampus, corpus striatum, nucleus accumbens, and olfactory nuclei (albeit, lower concentrations than at 1 hr). The AV nucleus of the thalamus has lesser radioactivity than in the remainder of the thalamus. Radioactivity in the remaining structures is negligible. By 5 hr (Fig. 5C), radioactivity in all structures has cleared substantially: 90% as estimated by relative gray levels. The radioactivity in the choroid plexus in this study with (R,S)-4IQNB has also been observed with similar studies using the (R,R)-isomer (*13*), but is not related to m-AChR.

The venous blood-radioactivity-curves for (R,S)-4IQNB and (R,R)-4IQNB are presented in Figure 6A. The curves were corrected for hydrophilic metabolites (Fig. 6B) by extracting plasma with EtOAc, in which the lipophilic forms of radioactivity are extracted (*7*). (R,R)- and (R,S)-4IQNB are 100% extracted when radioactivity is added to plasma in vitro. The slower clearance of total radioactivity by the (R,S)-diastereomer indicates slower clearance of the hydrophilic metabolites, rather than a difference in the rate of metabolism of the (R,S)- and (R,R)-diastereomers. The EtOAc extract from plasma at 3 hr postinjection was chromatographed and found to be heterogenous (Fig. 7). The lipophilic metabolites represented 12% of the extracted radioactivity in the case of (R,R)-4IQNB, but 20% in

TABLE 1
Systemic Distribution of [^{125}I] (R,S)-4IQNB in Rat

Tissue	% Injected dose/g* Time (hr) 0.25	0.5	1	2	4	6	24
Heart	0.742 (1.18)‡	0.582 (6.43)	0.334 (7.00)	0.151	0.080 (3.19)	0.050	<0.01† (0.408)
Blood	0.066 (0.054)	0.140 (0.072)	0.163	0.085	0.116 (0.045)	0.109 (0.065)	0.030
Femur	0.054 (0.018)	0.142 (0.106)	0.127 (0.051)	0.036	0.021 (0.016)	0.153 (0.026)	<0.01 (<0.01)
Muscle	0.105 (0.045)	0.263 (0.154)	0.181 (0.146)	0.119	0.044 (0.042)	0.100 (0.120)	<0.01 (<0.01)
Kidneys	1.22 (0.243)	1.01 (0.612)	0.681 (0.790)	0.351	0.280 (0.497)	0.167 (0.571)	<0.01 (<0.01)
Adrenals	1.98 (0.247)	1.47 (0.688)	0.825 (0.726)	0.344	0.137 (0.464)	0.077 (0.760)	<0.01 (<0.01)
Ovaries	0.767 (0.114)	0.872 (0.372)	0.695 (0.377)	0.289	0.102 (0.192)	0.156 (0.565)	<0.01
Liver	0.993 (0.091)	1.45	1.27 (0.219)	0.821	0.452 (0.144)	0.373 (0.107)	0.149 (0.077)
Lung	2.69 (0.214)	5.81 (0.326)	2.97 (0.460)	1.62	0.608 (0.367)	0.381 (0.345)	0.015 (0.164)
Jejunum	0.559 (0.296)	0.740 (1.81)	0.461 (1.71)	0.252	1.36 (1.41)	1.75 (3.65)	0.096 (0.650)

* Average of at least five animals, coefficient of variation < 20% for all organs.
† Count-rate not significantly above background.
‡ %-dose/g of [^{3}H]QNB coinjected with 4IQNB for comparison. Average of five animals with coefficient of variation <20% for all organs.

the case of the (R,S)-diastereomer. No attempt has been made to identify the additional peaks, but neither appears in chromatograms of radioactivity extracted from brain homogenates.

DISCUSSION

In this report, we present the characteristics of (R,S)-4IQNB. This isomer exhibits a high affinity for the m-AChR which is, however, threefold less than that of the (R,R)-diastereomer. By contrast, the in vitro kinetics of association and dissociation of (R,S)-4IQNB are faster by 2.5-fold and 13-fold, respectively, than observed with (R,R)-4IQNB. Clearance of the (R,S)-isomer in vivo from receptor-rich structures in the CNS is also more rapid than observed with (R,R)-4IQNB (*2,12,14*). After correcting for hydrophilic metabolites in the plasma, the plasma-radioactivity curves indicate that (R,R)- and (R,S)-4IQNB are metabolized at similar rates. Since the physicochemical properties of the diastereomers are the same and the clearance of the two radioligands from plasma are the same, the more rapid washout of radioactivity from the CNS in vivo should reflect the more rapid dissociation rate from the receptor.

The distribution of radioactivity in the CNS following i.v. injection provides an indication of the localization which would be observed in a tomographic study. The similarity in CNS localization between (R,S)- and (R,R)-4IQNB and the success in imaging human CNS with the (R,R)-diastereomer indicates the potential for imaging with [^{123}I] (R,S)-4IQNB. The distribution of (R,S)-4IQNB at 1 hr is directly proportional to the concentration of receptors in the structures shown in these sagittal slices (Fig. 5 and Table 2): corpus striatum > cortex=hippocampus > thalamus = colliculi > hypothalamus > cerebellum (*15–20*). The correspondence between receptor concentration and localization could result from saturation of the receptors in the CNS. For example, Fig. 5A presents the same binding pattern as that presented in Fig. 5C of Mash and Potter (*18*) for in vitro binding using [^{3}H] QNB. We have not explicitly determined the %-saturation in the studies using 0.5 mCi of 4IQNB, but <1% of the dose localizes in rat brain when 5 μCi of [^{125}I] (R,R)-4IQNB is injected (*2*). Assuming similar localization with 0.5 mCi, 5 pmol of radioligand would be present in the brain. The average concentration of receptor in the brain is 5×10^{-8} *M*, or 50 pmol per gram. Therefore, no more than 10% of the receptors would be occupied in these studies.

An alternative explanation is that the kinetic parameters which mediate localization may be such that radioligand localization is predominantly receptor-mediated, i.e., not predominantly a function of flow or diffusion. In studies on the compartmental analysis of (R,R)-4IQNB in rat, Sawada et al. (*7*) provides esti-

TABLE 2
Distribution of [^{125}I] (R,S) 4IQNB in Brain of Rat

Tissue	% Injected dose/g*						
	0.25	0.5	1	2	4	6	24
Cortex	0.154	0.259	0.269	0.153	0.076	0.0110	<0.01†
	(0.079)‡	(0.515)	(0.498)		(0.390)	(0.585)	(0.551)
Corpus striatum	0.139	0.242	0.288	0.140	0.073	0.115	<0.01
	(0.070)	(0.530)	(0.455)		(0.420)	(0.536)	(0.576)
Hippocampus	0.114	0.227	0.264	0.152	0.074	0.128	<0.01
	(0.064)	(0.455)	(0.389)		(0.340)	(0.475)	(0.470)
Thalamus	0.103	0.169	0.163	0.062	0.024	0.026	<0.01
	(0.061)	(0.455)	(0.389)		(0.320)	(0.450)	(0.400)
Superior colliculi	0.113	0.157	0.144	0.071	0.018	<0.01	<0.01
	(0.077)	(0.440)	(0.426)		(0.380)	(0.497)	(0.434)
Inferior colliculi	0.101	0.170	0.110	0.082	0.014	<0.01	<0.01
	(0.073)	(0.525)	(0.471)		(0.460)	(0.478)	(0.456)
Cerebellum	0.088	0.105	0.067	0.034	0.006	<0.01	<0.01
	(0.054)	(0.266)	(0.288)		(0.210)	(0.287)	(0.136)

* Average of at least five animals, coefficient of variation <20% for all organs.
† Count-rate not significantly above background.
‡ %-dose/g of [^{3}H]QNB coinjected with 4IQNB for comparison. Average of at least five animals, coefficient of variation < 20% for all structures.

mates of the pharmacokinetic parameters which indicate that radioligand localization is partially a function of the concentration of receptor, i.e., k_3 is not greater than k_2 (*21*), and that compartmental modeling provides binding potentials which strongly correlate with receptor concentrations (*7,13*).

The distribution of (R,S)-4IQNB determined autoradiographically shows that radioactivity dissociates from different structures at different rates. The rapid clearance of radioactivity from the thalamus, hypothalamus, colliculi, brain stem, and cerebellum relative to the cortex, hippocampus, and corpus striatum, may result from either the lower concentration of receptor in these structures (*22,23*) or the relative concentrations of the various receptor subtypes in the structures. We have shown with (R,R)-4IQNB that structures with the

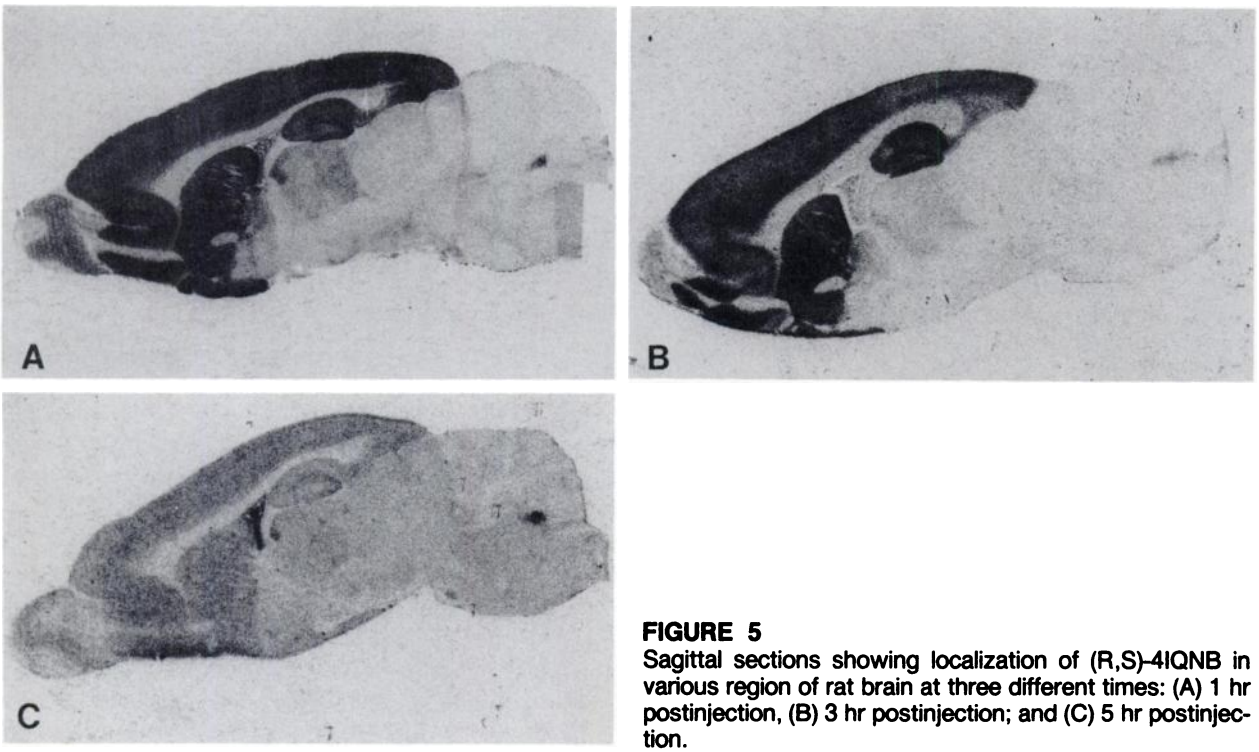

FIGURE 5
Sagittal sections showing localization of (R,S)-4IQNB in various region of rat brain at three different times: (A) 1 hr postinjection, (B) 3 hr postinjection; and (C) 5 hr postinjection.

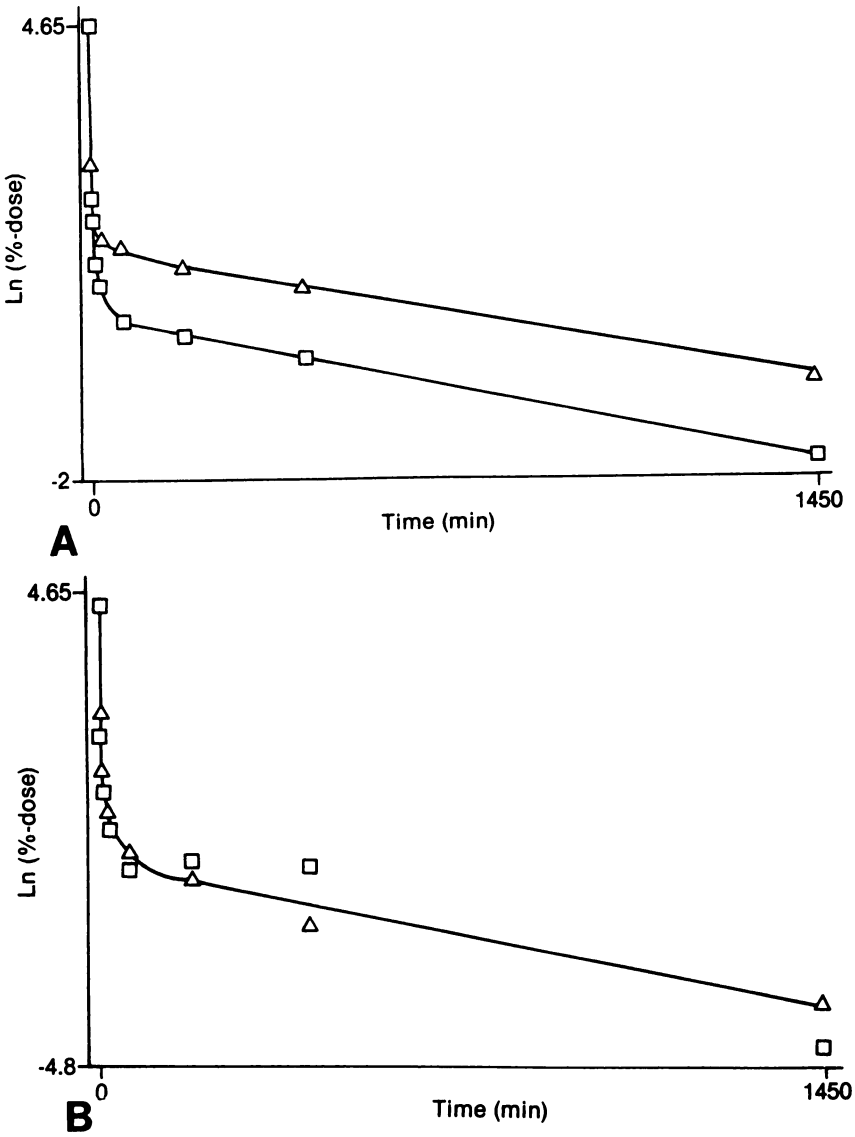

FIGURE 6
A: Blood-clearance of [^{125}I] (R,S)-4IQNB (△) and (R,R)-4IQNB (□) following a bolus injection of 0.1 mCi of radioactive ligand. B: Plasma clearance curves following correction for hydrophilic metabolites.

highest proportion of receptor subtypes which exhibit more rapid in vitro dissociation kinetics also exhibit more rapid in vivo clearance (*13,14*). The only difference in the results with the (R,R)- and (R,S)-isomers is the time course: the distribution with (R,S)-4IQNB at 3 hr postinjection is not observed with the (R,R)-diastereomer until 24 hr postinjection.

Results obtained from the AV nucleus of the thalamus provides evidence that equilibrium is approached with (R,S)-4IQNB by 5 hr. The concentration of receptor in the AV nucleus is higher than that of other thalamic nuclei visualized in Figure 5, but of a subtype exhibiting very rapid dissociation kinetics. Thus (R,S)-4IQNB clears more rapidly from this structure despite the concentration of m-AChR. At 5 hr, radioactivity in the AV nucleus is again higher than the other thalamic nuclei (Fig. 5C), though the total activity in the thalamus is much lower than at 1 hr. This result would be obtained if equilibrium conditions existed.

CONCLUSION

The localization of (R,S)-4IQNB is similar to that of (R,R)-4IQNB with the exception that the kinetics of interaction are more rapid. Although we did not observe a more rapid rate of localization with the (R,S)-isomer since we did not attempt to define the washin curve, we clearly observe a more rapid washout of radioactivity from the CNS, consistent with the faster in vitro dissociation rate. The more rapid kinetic properties of this isomer of 4IQNB should provide greater options in the design of imaging protocols for the determination of receptor concentrations in man. For example, quantitation of receptor concentration by virtue of receptor dissociation (*23*) should be facilitated by the more rapid kinetics of this isomer. The pharmacokinetics of this receptor-binding-radiotracer may also be appropriate for an "equilibrium" approach for receptor quantitation (*24,25*). Lastly, should kinetic studies be necessary for

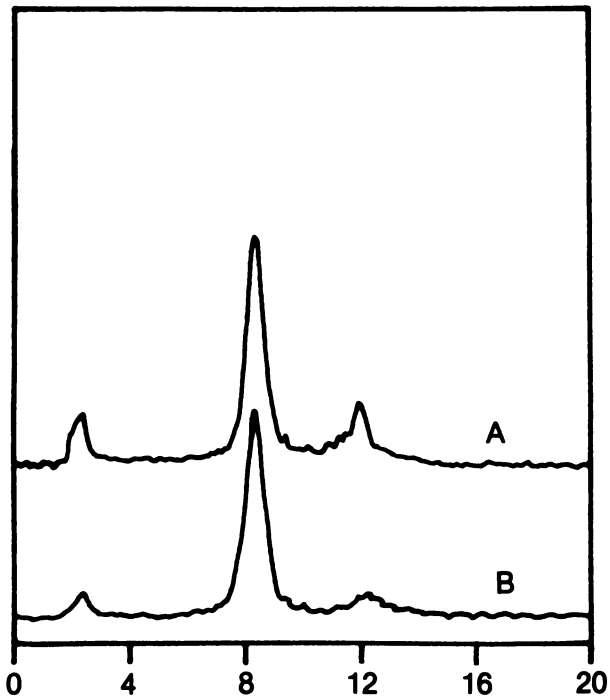

FIGURE 7
Chromatography of ethyl acetate extracts of plasma activity after 3 hrs following i.v. injection of 0.3 mCi of activity. (A) [^{125}I] (R,S)-4IQNB and (B) (R,R)-4IQNB. Chromatograms were obtained using silica gel plates developed in MeOH containing 2% NH_4OH.

the quantitation of receptor concentration, the existence of a compound with the same physicochemical properties as (R,R)-4IQNB, but different kinetic parameters can be used to test the validity of the kinetic models.

ACKNOWLEDGMENTS

The authors acknowledge the technical assistance of R. Getz on the autoradiographic studies and B. Francis for providing the TLC radiotraces for hydrophilic metabolites. This work was supported in part by Grant NS22255 from the National Institutes of Health, DHEW, and contract DE AS05 82ER60039 from the Department of Energy.

REFERENCES

1. Rzeszotarski WJ, Eckelman WC, Francis BE, et al. Synthesis and evaluation of radioionated derivatives of 1-azabicyclo(2.2.2)oct-3-yl-α-hydroxy-α-(4-iodophenyl)-α-phenylaetate as potential radiopharmaceuticals. *J Med Chem* 1984; 27:156–160.
2. Gibson RE, Weckstein DJ, Jagoda EJ, et al. The characteristics of I-125 4IQNB and H-3 QNB in vivo and in vitro. *J Nucl Med* 1984; 25:214–222.
3. Eckelman WC, Reba RC, Rzeszotarski WJ, et al. External imaging of cerebral muscarinic acetylcholine receptors. *Science* 1984; 223:291–293.
4. Holman LB, Gibson RE, Hill TC, et al. Muscarinic acetylcholine receptors in Alzheimer's disease. In vivo imaging with iodine-123-labeled 3-quinuclidinyl 4-iodobenzilate and emission tomography. *J Am Med Assoc* 1986; 254:3063–3066.
5. Meyerhoffer A. Absolute configuration of 3-quinuclidinyl benzilate and the behavioral effect in the dog of the optical isomers. *J Med Chem* 1972; 15:994–995.
6. Eckelman WC, Eng R, Rzeszotarski WJ, et al. Use of 3-quinuclidinyl 4-iodobenzilate as a receptor-binding radiotracer. *J Nucl Med* 1985; 26:637–642.
7. Sawada Y, Hiraga S, Francis B, et al. Kinetic analysis of 3-quinuclidinyl 4-[^{125}I]iodobenzilate transport and specific binding to muscarinic acetylcholine receptor in rat brain in vivo. *J Cereb Blood Flow Metab* 1989: in press.
8. Inch TD, Green DM Thompson PBJ. The central and peripheral activities of anti-cholinergic drugs. Some concepts of practical relevance. *J Pharm Pharmacol* 1973; 25:359–370.
9. Cohen VI, Rzeszotarski WJ, Gibson RE, et al. Preparation and properties of (R)-(−)-1-azabicyclo[2.2.2] oct-3-yl (R)-(+)-α-hydroxy-α-(4-[^{125}I]iodophenyl)-α-phenyl acetate and (R)-(−)-1-azabicyclo[2.2.2]oct-3-yl (S)-(−)-α-hydroxy-α-(4-[^{125}I]iodophenyl)-α-phenyl acetate as potential radiopharmaceuticals. *J Pharm Sci* 1989: in press.
10. Gibson RE, Rzeszotarski WJ, Jagoda EJ, et al. [^{125}I] 3-quinuclidinyl 4-iodobenzilate: a high affinity, high specific activity radioligand for the M_1 and M_2-acetylcholine receptors. *Life Sci* 1984; 34:2287–2292.
11. Eldridge JS, Crowther P. Absolute determination of I-125. *Nucleonics* 1964; 22:56–59.
12. Paxinos G, Watson C. The rat brain in stereotaxic coordinates. New York: Academic Press, 1986: Fig. 81.
13. Gibson RE. Imaging and quantification of muscarinic acetylcholine receptors. In: Frost JJ, Wagner HN, Jr. Neuroreceptor localization and quantification by positron-emission-tomography. Boston: Raven Press, 1989: in press.
14. Gibson RE, Moody T, Rzeszotarski WJ, Schneidau TS, Jagoda EM, Reba RC. Classification of M1 and M2 receptor subtypes in vivo by autoradiography using (^{125}I) (R,R) 4IQNB: implications for imaging receptor subtypes. *J Nucl Med* 1985; 25:P121.
15. Kobayashi RM, Palkovits M, Hruska RE, Rothschild R, Yamamura HI. Regional distribution of muscarinic cholinergic receptors in rat brain. *Brain Res* 1978; 154:13–21.
16. Wamsley JK, Zarbin MA, Birdsall NJM, Kuhar MJ. Muscarinic cholinergic receptors: autoradiographic localization of high and low affinity agonist binding sites. *Brain Res* 1980; 200:1–12.
17. Wamsley JK, Gehlert DR, Roeske WR, Yamamura HI. Muscarinic antagonist binding site heterogeneity as evidenced by autoradiography after direct labeling with [^{3}H]-QNB and [^{3}H]-pirenzepine. *Life Sci* 1984; 34:1395–1402.
18. Mash DC, Potter LT. Autoradiographic localization of M1 and M2 muscarinic receptors in the rat brain. *Neurosci* 1986; 19:551–564.
19. Cortes R, Palacios JM. Muscarinic cholinergic receptor subtypes in the rat brain. I. Quantitative autoradiographic studies. *Brain Res* 1986; 362:227–238.

20. Frey KA, Ehrenkaufer RLE, Agranoff BW. Quantitative in vivo receptor binding. II. Autoradiographic imaging of muscarinic cholinergic receptors. *J Neurosci* 1985; 5:2407–2414.
21. Zeeberg B, Wagner HN, Jr. Analysis of three- and four-compartment models for in vivo radioligand-neuroreceptor interaction. *Bull Math Biol* 1987; 49:469–486.
22. Frost JJ, Wagner HN, Jr. Kinetics of binding to opiate recepters in vivo predicted from in vitro parameters. *Brain Res* 1984; 305:1–11.
23. Gibson RE, Zeeberg B, Melograna Wang TF, Reba RC. Determination of regional receptor concentrations via radioligand dissociation kinetics. *J Nucl Med* 1985; 25(suppl):170.
24. Farde L, Hall H, Ehrin E, Sedvall G. Quantitative analysis of D-2 dopamine receptor binding in the living human brain by PET. *Science* 1986; 231:258–260.
25. Zeeberg B, Gibson R, Reba R. Accuracy of in vivo neuroreceptor quantification by PET and review of steady-state, transient, double-injection, and equilibrium models. *IEEE Trans Med Imag* 1988; 7:203–212.